Structural Diversity of the Epigenetics Pocketome

Alexandre Cabaye[1,$], Kong T Nguyen[1,#], Lihua Liu[1], Vineet Pande[2], Matthieu Schapira[1,3,*]

[1] Structural Genomics Consortium, 101 College street, University of Toronto, Toronto, ON, M5G 1L7, Canada

[2] Discovery Sciences, Janssen Pharmaceutical Companies of Johnson & Johnson, Turnhoutseweg 30, 2340 Beerse, Belgium

[3] The Department of Pharmacology and Toxicology, University of Toronto, Toronto, ON, M5S 1A8, Canada

[$]Present address: Université Paris Diderot, 35 rue Hélène Brion, 75205 Paris, France

[#]Present address: Proteorex Therapeutics Inc.,100 College street, suite 302, Toronto, ON M5G 1L5, Canada

*To whom correspondence should be sent: matthieu.schapira@utoronto.ca

Short Title: Diversity of the Epigenetics Pocketome

Keywords: epigenetics; chromatin factors; binding pocket; drug design; pocketome; inhibitor; selectivity; structure.

ABSTRACT

Protein families involved in chromatin-templated events are emerging as novel target classes in oncology and other disease areas. The ability to discover selective inhibitors against chromatin factors depends on the presence of structural features that are unique to the targeted sites. To evaluate challenges and opportunities towards the development of selective inhibitors, we calculated all pair wise structural distances between 575 structures from the protein databank representing 163 unique binding pockets found in protein domains that write, read or erase post-translational modifications on histones, DNA and RNA. We find that the structural similarity of binding sites does not always follow the sequence similarity of protein domains. Our analysis reveals increased risks of activity across target-class for compounds competing with the cofactor of protein arginine methyltransferases, lysine acetyltransferases and sirtuins, while exploiting the conformational plasticity of a protein target is a path towards selective inhibition. The structural diversity landscape of the epigenetics pocketome can be explored via an open-access graphic user interface at thesgc.org/epigenetics_pocketome.

INTRODUCTION

Epigenetic mechanisms control gene expression profile and cell fate in response to environmental and chemical cues. This complex regulation machinery relies mainly on the chemical modification of DNA and histone proteins at specific genomic loci[1,2]. RNA methylation is also emerging as a mechanism to regulate miRNA-mediated control of transcription[3,4]. These post-translational modifications are written, read and erased by catalytic and binding domains found in chromatin factors. Pharmacological targeting of these structural protein modules is an emerging therapeutic strategy in cancer and potentially other disease areas[5]: DNA methyltransferase (DNMT) and histone deacetylase (HDAC) inhibitors are approved against myelodysplatic syndrome, leukemia and lymphoma[6,7], while inhibitors of protein methyltransferases (PMT) and bromodomains – binding modules that read acetylated lysines on histone tails – are in Phase II or III clinical trials[8].

The development of potent and selective inhibitors of chromatin factors has become the focus of intense effort in the drug discovery community. Selective inhibition relies on the structural uniqueness of the targeted binding site. Appreciation of the structural diversity of a given binding pocket across an entire target class can reveal which are the most similar binding sites, and where are the main risks of off target activity.

We have analyzed the structural diversity of all currently known targetable binding pockets across twenty epigenetic target classes for which a structure is available. The resulting landscape of the epigenetic pocketome highlights differences between sequence similarity of protein domains and structural diversity of binding pockets, and reveals

unexpected variability in the structural diversity of cofactor binding sites from one target class to another. Gene-specific data is available to the community in an open access format through an online interface at thesgc.org/epigenetics_pocketome/.

MATERIALS AND METHODS

Database assembly

All structures of epigenetic target classes were retrieved from the Chromohub database[9]. A script in ICM (Molsoft LLC, San Diego) was used to automatically filter-out structures where the pocket was not occupied by chemical matter (substrate, inhibitor, molecule from the crystallization buffer): all structures were automatically aligned onto representative template structures with a bound ligand for each target class; target structures were kept only when a bound molecule was found within 1 Å from the reference ligand.

Calculation of structural distances between pockets

The ICM atomic property field method was used to calculate structural distances between any two pockets[10]. Pockets are defined as the ensemble of atoms within 5.5Å of the bound ligand. Since the nature of the ligand has an impact on the definition of the pocket, ligands from the native structures were replaced with reference ligands that were unique to a target class or phylogenetic subfamily. These reference ligands were generally methylated or acetylated lysine or arginine. Two exceptions were bromodomains, where the benzodiazepine JQ1 was used as it better occupies the binding site, and KDMs, where

we found that an artificial ligand composed of a lysine flanked by 2 glycines better occupied the pocket.

Distance normalization

To make sure that relative structural distances (D_{APF}) could be compared within each target class, APF distances (E_{APF}) were normalized as previously described [10]:

$S_{APF} = -\tanh((E_{APF} - E0)/\Delta 0)$, where $E0 = -250$ & $\Delta 0 = 100$

$D_{APF}(A,B) = S_{APF}(A,A) + S_{APF}(B,B) - 2\,S_{APF}(A,B)$

Graphic user interface

Phylogenetic tree generation and data mapping on the trees were carried-out using the technology previously described for Chromohub[9].

RESULTS AND DISCUSSION

Structural Coverage

Current reversible inhibitors of chromatin factors are competing with either the cofactor-, the substrate- or the ligand-binding site of their targets[5]. We collected from the protein databank (PDB) the structures of binding pockets from human protein domains that write, read or erase methyl or acetyl marks on histones, DNA and RNA. To ensure that the analyzed pockets were not partially occluded by misfolded side-chains, we only kept pockets occupied by chemical matter (substrate, natural ligand such as methyl-lysine

(Kme), cofactor, inhibitor, or molecule from the crystallization buffer). When multiple structures were available for a given pocket, all were kept.

The resulting collection is composed of 575 structures representing 163 unique binding pockets (Figure 1 and Supplementary Table S1). Included are the Kme binding site of 48 Kme reader domains, the acetyl-lysine (Kac) binding site of 21 bromodomains, the cofactor (S-adenosylmethionine - SAM) binding site of 27 PMTs, 15 RNA-methyltransferases (RNMTs), and 2 DNMTs, the substrate lysine or arginine binding pocket of 11 PMTs and 10 lysine demethylases (KDMs), the cofactor (acetyl-CoA) and substrate (lysine) binding pocket of 8 and 2 lysine acetyltransferases (KATs) respectively, the substrate (Kac) binding site of 4 HDACs, and the cofactor (nicotinamide-adenine dinucleotide – NAD) site of 5 sirtuins (SIRTs). Compounds occupying allosteric sites of two PMTs have also been reported[11] (PDB code 4QPP), and these pockets were also included (Supplementary Table S1, Figure 1).

Validation of computed structural distances

Structural distances between all binding pockets were calculated by the atomic property fields method implemented in ICM[10]. Briefly, continuous pharmacophoric properties derived from atoms within 5.5Å of the bound ligand are compared between any two given binding pockets (see methods section for details). This method was applied in the past to successfully cluster in a blind experiment all ligand-binding pockets in the PDB[10].

To test the relevance of this approach, we measured structural distances between the Kac binding pockets of HDAC2 (a class I HDAC) as well as HDAC4 (a class IIa HDAC) with all other pockets in the database. Class IIa HDACs only have residual catalytic activity

due to the substitution of a catalytic tyrosine with a histidine, resulting in significant alteration in the structural chemistry of the binding site (Figure 2)[12,13]. Indeed, we find that the substrate pocket of HDAC8, another class I HDAC, is significantly closer to HDAC2 (structural distance SD=0.18) than class IIa HDACs (SD > 0.7) while the pocket of HDAC7, a class IIa enzyme, is closer to HDAC4 (SD=0.34) than class I HDACs (SD > 0.88) (Figure 2).

The cofactor site of PMTs was used a second validation experiment. PMTs can be divided into two phylogenetic groups: SET domain methyltransferases, and Rossman fold methyltransferases. Both groups of enzymes use SAM as a methyl-donating cofactor. The bound conformation of SAM is conserved within each subfamily of PMT, but distinct between the two families, which implies greater structural diversity in the SAM pocket between the two groups[14,15]. Indeed, we find that structural distances from the cofactor binding pocket of the SET domain PMT EHMT2/G9a are less than 0.75 for all SET domain methyltransferases (with the exception of SMYD1: SD=0.86), while PRMTs, DOT1L and other Rossman fold methyltranserases have SD values greater than 1.5 (Figure 2): off-target effects of SAM competitors can be avoided between PRMTs and SET domain methyltransferases.

Sequence conservation does not always dictate pocket similarity

Chances of off-target activity of an inhibitor are expected to increase with binding domain sequence similarity. This trend can be observed for instance on the phylogenetic tree of bromodomains. Kac binding pockets found in the BET bromodomain phylogenetic subfamily (BRD2, BRD3, BRD4, and BRDT) are structurally close (0.03 <

SD < 0.25) to the Kac binding pocket of BRD4(1) (first bromodomain of BRD4), while pockets found on non-BET bromodomains are more distant (0.5 > SD > 1.89) (Figure 3). This is in agreement with the observation that current BRD4 bromodomain inhibitors, some in the clinic, are poorly selective within the BET family[16].

An exception is the Kac binding pocket of CREBBP which is relatively close to the Kac pocket of BRD4(1) (SD=0.24), while the CREBBP bromodomain is not a close phylogenetic neighbour of BRD4(1) (31% sequence identity between the two bromodomains). Superimposing the structures of the BRD4(1) and CREBBP Kac binding pockets highlights a high structural similarity, the only significant difference being substitution of C136 in BRD4 for A1164 in CREBBP (Figure 3). This exception indicates that phylogenetic proximity does not necessarily correlate with binding pocket similarity. Further supporting this notion, we observe that while BPTF is closer to BRD4(1) than CREBBP in sequence (37% sequence identity between the bromodomains of BRD4(1) and BPTF), its binding pocket is more distant (SD= 0.97 between Kac binding pockets of BRD4(1) and BPTF) (Figure 3). Superimposing the BRD4(1) and BPTF structures highlights numerous important differences, including substitution of L92 in BRD4 with D101 in BPTF. Interestingly, we note that the only cross-activity observed for the BET bromodomain (i.e. BRD2, BRD3, BRD4, BRDT) inhibitor PFI-1 is with CREBBP/EP300 (thermal stabilization of 2-3 °C at 10 μM)[17], and the only cross-activity observed for CREBBP/EP300 bromodomain inhibitors is with BET bromodomains (thermal stabilization of 2-3 °C at 10 μM)[18]. This supports the notion that APF structural distances correlate with experimental selectivity profiles.

Together, these results show that sequence conservation generally but not always correlates with binding pocket similarity and off-target liability.

The SAM binding pocket is conserved in PRMTs and variable in RNMTs

PMT inhibitors currently in clinical trial (namely EZH2 and DOT1L inhibitors) are all competing with the cofactor SAM [8], and efforts are ongoing to target the cofactor binding pocket of other PMTs and other epigenetic target classes such as DNMTs or RNMTs. While the structural diversity of the SAM binding pocket was sufficient to develop highly specific EZH2 and DOT1L cofactor competitors, the chemical tractability of the cofactor site of other targets is unclear.

To evaluate the chances of designing specific cofactor competitors, we measured the structural diversity of the cofactor site of PMTs, RNMTs and DNMTs, which all use SAM as a cofactor (Figure 4). We find that as a group, PMTs, RNMTs and DNMTs have very variable SAM binding sites (median structural distance for the 903 pairs of SAM binding sites where structures are available: 2.7). This indicates that, while SAM binds to all these pockets, they are structurally divergent, and compounds that are not close mimetics of SAM have low chances of acting as pan-inhibitors. The fact that potent SAM-competing EZH2 or DOT1L inhibitors are inactive against other PMTs supports this result[19-21].

We find that the structural diversity is still high when considering PMTs only (median SD: 1.9). When focusing exclusively on SET domain PMTs, or exclusively on Rossman-fold PMTs, the median SD is lower, but still greater than 0.5, which indicates sufficient diversity to develop selective inhibitors. On the other hand, the median SD value

between the SAM binding sites of PRMTs drops below 0.05, indicating very high structural similarity (Figure 4). For instance, structural distances from the SAM site of CARM1 are below or equal to 0.01 for PRMT1, PRMT3 and PRMT6, and 0.1 for PRMT5 (Figure 5). Superimposing the SAM pockets of CARM1 and PRMT3 confirm a high structural similarity (Figure 5). Similarly, we find close similarity between the cofactor sites of DNMT1 and DNMT3A (SD=0.09).

The SAM binding site of RNMTs is much more diverse, as indicated by a median SD of 1.0 among the 91 pairs of genes with structures in the PDB (Figure 4). Superimposing the structures of MEPCE and METTL1, which are both on the same phylogenetic branch of the RNMT tree but separated by a structural distance of 0.31, clearly reveals extensive structural differences between the two SAM binding sites (Figure 5).

We therefore find little variation in the SAM binding pocket of PRMTs, and much greater diversity in RNMTs and SET domain PMTs. This indicates that finding selective SAM competitors will be more challenging for PRMTs than it has been for EZH2, and supports systematic screening of PRMT lead candidates against the entire target class to avoid unanticipated off-target effects.

Low structural variability at the cofactor pocket of SIRTs and KATs

Sirtuins - which have deacetylase activity - and acetyltransferases, two other target classes involved in epigenetic mechanisms, also rely on the recruitment of a cofactor, NAD and acetyl-coA respectively, at dedicated binding pockets. To evaluate the chances of developing selective cofactor competitors of SIRTs and KATs, we measured for each

of these protein family the structural distances separating all cofactor binding sites present in the PDB.

We find that both binding sites are very conserved (Figure 4). This is especially the case for the NAD pocket of SIRTs, where all pair wise structural distances are lower than 0.01, as illustrated by the superimposition of the SIRT1 and SIRT6 cofactor binding sites (Figure 4, Figure 6A). The acetyl-CoA pocket of KATs is also highly conserved (median SD across 36 pair wise distances < 0.1), and the only pocket that is significantly different is the cofactor binding site of EP300. All structural distances from the acetyl-coA site of HAT1 are lower than 0.05, except EP300 (SD=1.19). Conversely, all structural distances from the cofactor site of EP300 are greater than 0.35 (Figure 6 B,C). Overlaying structures clearly shows high structural similarity between the cofactor sites of HAT1 and KAT5, which are distant on the phylogenetic tree, but high structural divergence between the cofactor sites of EP300 and ATAT1, which are close on the phylogenetic tree (Figure 5B,C).

Together, these results indicate that developing selective NAD and acetyl-CoA competitors against SIRTs and KATs respectively is a challenging enterprise, with the exception of EP300, which has a distinct acetyl-CoA binding pocket.

Conformational dynamics can increase structural diversity

The structural plasticity of a binding pocket can sometimes be exploited to develop selective inhibitors: if a binding site can be remodeled in a conformation that is distinct from its substrate- or cofactor-bound state, compounds that occupy this altered state

should have less chances of binding the substrate or cofactor pocket of phylogenetic neighbours.

For instance, an activation loop is folding on the cofactor in the catalytically active state of the PMT DOT1L, but undergoes a dramatic conformational rearrangement upon binding of potent, selective DOT1L inhibitors. The compounds exploit the remodeled cofactor site, compete with the cofactor, and lock the enzyme in a catalytically inactive state [22,23]. The structural uniqueness of the remodeled DOT1L cofactor site translates in greater structural distances from the SAM binding pockets of other methyltransferases: while SAM-bound DOT1L has a structure that is relatively close to the cofactor site of the RNMT TGS1 (SD=0.08) (Figure 7A), the closest pocket from the remodeled cofactor site of DOT1L is the RNMT1 MEPCE, with a high SD of 0.43. Superimposing DOT1L and TGS1 structures confirms lower similarity with the remodeled conformation of DOT1L (Figure 7A,B).

We find that the pockets most similar to the cofactor site of DOT1L are equally found among RNMTs and PRMTs, but are not present in SET domain PMTs (Figure 7). This should come as no surprise, since DOT1L, PRMTs and RNMTs are all Rossman-fold methyltransferases, while SET domain PMTs are not. Intriguingly, the second closest pocket to the SAM site of DOT1L is the cofactor pocket of PRMT5. Although weak, this relative structural proximity is in agreement with the observed selectivity profile of the picomolar inhibitor of DOT1L EPZ004777, which was tested against 10 PMTs and had cross-reactivity only against PRMT5[21]. We also note that, as in the DOT1L structure, a flexible loop located next to the Rossman fold of PRMT5 is folding on the cofactor, suggesting that structural remodeling can also take place at the SAM pocket of PRMT5[24].

Structural plasticity is not unique to the cofactor site of DOT1L. Conformational dynamics at the post-SET secondary element of SET domain PMTs, and at the α-helix of PRMTs results in significant remodeling of both cofactor- and substrate-binding sites, and may translate in opportunities for the development of selective inhibitors[25,26].

As future structures better delineate the structural plasticity of the epigenetic pocketome, novel design strategies will surface for the development of potent and selective inhibitors.

Pocket similarity rationalizes epigenetic mark recognition

Recognition of specific post-translational modifications on histone side-chains by dedicated reader domains is central to the interpretation of the histone code[27]. Methylation of lysine and arginine residues are among the most common histone marks, and are read by a limited set of structural modules, including Tudor domains[28,29]. Aromatic cages composed of two to four aromatic side-chains positioned in an orthogonal arrangement act as sensors of methylated lysines and arginines (Rme)[28,30]. While aromatic cages found on PHD fingers, MBT, Chromo or PWWP domains are binding Kme, aromatic cages found on Tudor domains bind either Kme or Rme[31], and the structural basis for histone mark specificity is not clearly understood.

We find that all pockets closest to the aromatic cage of SMNDC1, a Rme binding site, are also Rme-binding aromatic cages found in Tudor domains, suggesting that well-defined structural features are underlying selective recognition of methylated arginines (Figure 8A). Comparison of Tudor-domain aromatic cages sensing Kme and Rme side-chains shows that the latter are systematically composed of four aromatic side-chains, two of which are positioned in a parallel orientation. Quite similar arrangements are found in

some of the Kme binding pockets, such as the TP53BP1 aromatic cage (which is why these Kme binding sites are almost as close to SMNDC1 as Rme binding pockets), but a distinctive feature of methyl-lysine binding pockets is that the two facing aromatic side-chains are in close proximity (< 7.7 Å between the center of the aromatic rings in all cases). This results in efficient stacking of the guanidinium group, sandwiched between the two facing aromatic rings. The distance is systematically larger (> 8.9Å) in methyl-lysine binding pockets, a necessity to accommodate a bulky methyl-ammonium group (Figure 8A).

These observations suggest that the structural diversity landscape of the epigenetics pocketome drawn in this work can provide some indications on the substrates recognized by reader domains.

In this regard, we find that the closest pocket to the Kme3-binding aromatic cage of the UHRF1 Tudor domain is the first MBT domain of L3MBTL (figure 8B). L3MBTL has three MBT domains; the second domain is known to act as Kme binding site, but no binding activity was reported for the first domain[32]. Superimposing the two structures confirms a very high similarity between the UHRF1 and L3MBTL binding sites (Figure 8B). It would be interesting to test biochemically whether the first MBT domain of L3MBTL can indeed bind Kme.

CONCLUSIONS

The structural diversity landscape of the epigenetic pocketome drawn here provides structural similarities between binding sites rather than sequence similarities between

protein domain sequences. This increased level of resolution is valuable to medicinal chemists and biochemists that design, test and profile chemical compounds targeting chromatin factors. This work reveals that cofactor sites of SET domain-PMTs and RNMTs are more diverse than those of PRMTs, KATs and sirtuins: compounds targeting the latter should be systematically profiled against the entire target class to identify probable off-target activity. Exploiting the structural plasticity of binding pockets (observed in numerous chromatin factors) can significantly increase the selectivity profile of inhibitors. Selective allosteric inhibition of an epigenetic target, PRMT3, was also reported and it will be interesting to see novel inhibitory mechanisms emerge in the future [11]. Finally, an online graphic user interface brings all the data generated in this work and future updates to the epigenetics community at thesgc.org/epigenetics_pocketome.

ACKNOWLEDGEMENTS

The SGC is a registered charity (no. 1097737) that receives funds from AbbVie, Bayer, Boehringer Ingelheim, Genome Canada through Ontario Genomics Institute Grant OGI-055, GlaxoSmithKline, Janssen, Lilly Canada, Merck, the Novartis Research Foundation, the Ontario Ministry of Economic Development and Innovation, Pfizer, Takeda, and Wellcome Trust Grant 092809/Z/10/Z. The authors declare no conflict of interest.

SUPPLEMENTARY INFORMATION

Supplementary Table S1, providing a list of the binding pockets and PDB structures used in this work, can be found in the online version of this article

REFERENCES

1. Jones PA. Functions of DNA methylation: islands, start sites, gene bodies and beyond. Nat Rev Genet 2012;13(7):484-492.
2. Kouzarides T. Chromatin modifications and their function. Cell 2007;128(4):693-705.
3. Xhemalce B, Robson SC, Kouzarides T. Human RNA methyltransferase BCDIN3D regulates microRNA processing. Cell 2012;151(2):278-288.
4. Nilsen TW. Molecular biology. Internal mRNA methylation finally finds functions. Science 2014;343(6176):1207-1208.
5. Arrowsmith CH, Bountra C, Fish PV, Lee K, Schapira M. Epigenetic protein families: a new frontier for drug discovery. Nat Rev Drug Discov 2012;11(5):384-400.
6. Stresemann C, Lyko F. Modes of action of the DNA methyltransferase inhibitors azacytidine and decitabine. Int J Cancer 2008;123(1):8-13.
7. Marks PA, Breslow R. Dimethyl sulfoxide to vorinostat: development of this histone deacetylase inhibitor as an anticancer drug. Nat Biotechnol 2007;25(1):84-90.
8. Copeland RA. Molecular pathways: protein methyltransferases in cancer. Clin Cancer Res 2013;19(23):6344-6350.
9. Liu L, Zhen XT, Denton E, Marsden BD, Schapira M. ChromoHub: a data hub for navigators of chromatin-mediated signalling. Bioinformatics 2012;28(16):2205-2206.
10. Totrov M. Ligand binding site superposition and comparison based on Atomic Property Fields: identification of distant homologues, convergent evolution and PDB-wide clustering of binding sites. BMC Bioinformatics 2011;12 Suppl 1:S35.
11. Siarheyeva A, Senisterra G, Allali-Hassani A, Dong A, Dobrovetsky E, Wasney GA, Chau I, Marcellus R, Hajian T, Liu F, Korboukh I, Smil D, Bolshan Y, Min J, Wu H, Zeng H, Loppnau P, Poda G, Griffin C, Aman A, Brown PJ, Jin J, Al-Awar R, Arrowsmith CH, Schapira M, Vedadi M. An allosteric inhibitor of protein arginine methyltransferase 3. Structure 2012;20(8):1425-1435.
12. Schapira M. Structural biology of human metal-dependent histone deacetylases. Handb Exp Pharmacol 2011;206:225-240.
13. Schuetz A, Min J, Allali-Hassani A, Schapira M, Shuen M, Loppnau P, Mazitschek R, Kwiatkowski NP, Lewis TA, Maglathin RL, McLean TH, Bochkarev A, Plotnikov AN, Vedadi M, Arrowsmith CH. Human HDAC7

harbors a class IIa histone deacetylase-specific zinc binding motif and cryptic deacetylase activity. J Biol Chem 2008;283(17):11355-11363.
14. Campagna-Slater V, Mok MW, Nguyen KT, Feher M, Najmanovich R, Schapira M. Structural chemistry of the histone methyltransferases cofactor binding site. J Chem Inf Model 2011;51(3):612-623.
15. Copeland RA, Solomon ME, Richon VM. Protein methyltransferases as a target class for drug discovery. Nat Rev Drug Discov 2009;8(9):724-732.
16. Filippakopoulos P, Knapp S. Targeting bromodomains: epigenetic readers of lysine acetylation. Nat Rev Drug Discov 2014;13(5):337-356.
17. Picaud S, Da Costa D, Thanasopoulou A, Filippakopoulos P, Fish PV, Philpott M, Fedorov O, Brennan P, Bunnage ME, Owen DR, Bradner JE, Taniere P, O'Sullivan B, Muller S, Schwaller J, Stankovic T, Knapp S. PFI-1, a highly selective protein interaction inhibitor, targeting BET Bromodomains. Cancer research 2013;73(11):3336-3346.
18. Hay DA, Fedorov O, Martin S, Singleton DC, Tallant C, Wells C, Picaud S, Philpott M, Monteiro OP, Rogers CM, Conway SJ, Rooney TP, Tumber A, Yapp C, Filippakopoulos P, Bunnage ME, Muller S, Knapp S, Schofield CJ, Brennan PE. Discovery and optimization of small-molecule ligands for the CBP/p300 bromodomains. J Am Chem Soc 2014;136(26):9308-9319.
19. McCabe MT, Ott HM, Ganji G, Korenchuk S, Thompson C, Van Aller GS, Liu Y, Graves AP, Della Pietra A, 3rd, Diaz E, LaFrance LV, Mellinger M, Duquenne C, Tian X, Kruger RG, McHugh CF, Brandt M, Miller WH, Dhanak D, Verma SK, Tummino PJ, Creasy CL. EZH2 inhibition as a therapeutic strategy for lymphoma with EZH2-activating mutations. Nature 2012;492(7427):108-112.
20. Knutson SK, Wigle TJ, Warholic NM, Sneeringer CJ, Allain CJ, Klaus CR, Sacks JD, Raimondi A, Majer CR, Song J, Scott MP, Jin L, Smith JJ, Olhava EJ, Chesworth R, Moyer MP, Richon VM, Copeland RA, Keilhack H, Pollock RM, Kuntz KW. A selective inhibitor of EZH2 blocks H3K27 methylation and kills mutant lymphoma cells. Nature chemical biology 2012;8(11):890-896.
21. Daigle SR, Olhava EJ, Therkelsen CA, Majer CR, Sneeringer CJ, Song J, Johnston LD, Scott MP, Smith JJ, Xiao Y, Jin L, Kuntz KW, Chesworth R, Moyer MP, Bernt KM, Tseng JC, Kung AL, Armstrong SA, Copeland RA, Richon VM, Pollock RM. Selective killing of mixed lineage leukemia cells by a potent small-molecule DOT1L inhibitor. Cancer Cell 2011;20(1):53-65.
22. Yu W, Chory EJ, Wernimont AK, Tempel W, Scopton A, Federation A, Marineau JJ, Qi J, Barsyte-Lovejoy D, Yi J, Marcellus R, Iacob RE, Engen JR, Griffin C, Aman A, Wienholds E, Li F, Pineda J, Estiu G, Shatseva T, Hajian T, Al-Awar R, Dick JE, Vedadi M, Brown PJ, Arrowsmith CH, Bradner JE, Schapira M. Catalytic site remodelling of the DOT1L methyltransferase by selective inhibitors. Nat Commun 2012;3:1288.
23. Basavapathruni A, Jin L, Daigle SR, Majer CR, Therkelsen CA, Wigle TJ, Kuntz KW, Chesworth R, Pollock RM, Scott MP, Moyer MP, Richon VM, Copeland RA, Olhava EJ. Conformational adaptation drives potent, selective and durable inhibition of the human protein methyltransferase DOT1L. Chem Biol Drug Des 2012;80(6):971-980.

24. Antonysamy S, Bonday Z, Campbell RM, Doyle B, Druzina Z, Gheyi T, Han B, Jungheim LN, Qian Y, Rauch C, Russell M, Sauder JM, Wasserman SR, Weichert K, Willard FS, Zhang A, Emtage S. Crystal structure of the human PRMT5:MEP50 complex. Proceedings of the National Academy of Sciences of the United States of America 2012;109(44):17960-17965.
25. Schapira M, Ferreira de Freitas R. Structural biology and chemistry of protein arginine methyltransferases. Med Chem Commun 2014;5:1779-1788.
26. Schapira M. Structural Chemistry of Human SET Domain Protein Methyltransferases. Curr Chem Genomics 2012;5(Suppl 1):85-94.
27. Fischle W, Wang Y, Allis CD. Binary switches and modification cassettes in histone biology and beyond. Nature 2003;425(6957):475-479.
28. Taverna SD, Li H, Ruthenburg AJ, Allis CD, Patel DJ. How chromatin-binding modules interpret histone modifications: lessons from professional pocket pickers. Nat Struct Mol Biol 2007;14(11):1025-1040.
29. James LI, Frye SV. Targeting chromatin readers. Clin Pharmacol Ther 2013;93(4):312-314.
30. Gao C, Herold JM, Kireev D, Wigle T, Norris JL, Frye S. Biophysical probes reveal a "compromise" nature of the methyl-lysine binding pocket in L3MBTL1. J Am Chem Soc 2011;133(14):5357-5362.
31. Lu R, Wang GG. Tudor: a versatile family of histone methylation 'readers'. Trends Biochem Sci 2013;38(11):546-555.
32. Min J, Allali-Hassani A, Nady N, Qi C, Ouyang H, Liu Y, MacKenzie F, Vedadi M, Arrowsmith CH. L3MBTL1 recognition of mono- and dimethylated histones. Nat Struct Mol Biol 2007;14(12):1229-1230.

FIGURE LEGENDS:

Figure 1: Structural coverage of the epigenetics pocketome. The ensemble of structures collected in the PDB covers 163 binding pockets (highlighted in red) across 18 classes of protein domains that write, read and erase post-translational modifications on histones, DNA and RNA.

Figure 2: Structural distances accurately distinguish Class I from Class II HDACs, as well as SET-domain from Rossman fold SAM pockets. Structural distances from the Kac binding pocket of HDAC2 (top left), and HDAC4 (top right) are mapped on a phylogenetic tree of the HDAC family. Structural distances from the cofactor binding pocket of EHMT2/G9a are mapped on the phylogenetic trees of SET-domain and Rossman-fold PMTs (bottom). Structural differences between the Kac binding pockets of Class I and Class II HDACs are shown (PDB codes are HDAC2: 4LXZ, HDAC4:2VQM, HDAC7:3C0Z, HDAC8:1T69).

Figure 3: Pockets from phylogenetically distant isoforms are not necessarily the most distant structurally. Structural distances from the Kac binding pocket of BRD4's first bromodomain are mapped on a phylogenetic tree. Structural differences between the Kac site of BRD4(1) and CREBBP (left) or BPTF (right) are highlighted. When multiple bromodomains are present in a protein, the bromodomain number is indicated in parenthesis.

Figure 4: Structural diversity landscape of cofactor binding pockets. The distribution of minimum pair wise distances separating all pockets with holo-structures in the PDB is shown as boxplots for cofactor binding sites of epigenetic target classes. An estimate of

the minimum distance necessary to develop selective inhibitors is indicated with a dashed horizontal bar. When several structure of the same pocket are present in the PDB, all distances are calculated and only the minimum distance is used. The number of minimum distances is indicated in parenthesis.

Figure 5: The structural diversity of the SAM binding site varies from one target class to another. (A) Structural distances from the SAM binding pocket of CARM1 are mapped on a phylogenetic tree of Rossman fold PMTs (top); the few structural differences between the SAM pockets of CARM1 (PDB: 4IKP) and PRMT3 (PDB: 2FYT) are shown (bottom). (B) Structural distances from the SAM binding pocket of the RNMT MEPCE are mapped on a phylogenetic tree of RNMTs (top); the large structural differences between the SAM pockets of MEPCE (PDB: 3G07) and METTL1 (PDB: 3CKK) are shown (bottom).

Figure 6: Low structural diversity at the cofactor site of SIRTs and KATs. (A) Structural distances from the NAD binding pocket of SIRT1 are mapped on a phylogenetic tree of human SIRTs (top); the few structural differences between the NAD pockets of phylogenetically distant SIRT1 and SIRT6 are shown (bottom). (B) Structural distances from the acetyl-CoA binding pocket of HAT1 are mapped on a phylogenetic tree of KATs (top); the few structural differences between the acetyl-CoA pockets of HAT1 (PDB: 2POW) and KAT5 (PDB: 2OU2) are shown (bottom). (C) Structural distances from the acetyl-CoA binding pocket of EP300 are mapped on a phylogenetic tree of KATs (top); the numerous structural differences between the acetyl-CoA pockets of EP300 (PDB: 4PZR) and ATAT1 (PDB: 4GS4) are shown (bottom).

Figure 7: Altered pocket conformation increases structural diversity. (A) Structural distances of SAM binding sites from the cofactor pocket of DOT1L bound to SAM are listed (left) and outlined on phylogenetic trees (right). The structural similarity between the cofactor-bound pockets of DOT1L (PDB: 1NW3) and TGS1 (PDB: 3GDH) is detailed. (B) Structural distances of SAM binding sites from the remodeled conformation of the DOT1L cofactor site in complex with the selective inhibitor EPZ004777 (PDB: 4ER5). Table and figures as above.

Figure 8: Pocket similarity correlates with histone mark recognition. (A-left): Kme and Rme binding pockets from Tudor domains are listed along their structural distances to the Rme binding site of SMNDC1. (A-right): Structure of aromatic cages from Tudor domains in complex with Rme and Kme. PDB codes: SMN1 [4A4E], SND1[3OMC], TDRD3[3PMT], UHRF1[4GY5], TP53BP1[3LGL], MSL3L1[3OA6]. (B-left): pockets structurally closest to the Kme binding pocket of the UHRF1 Tudor domain. (B-right): structures from the aromatic cages of the UHRF1 Tudor domain [4GY5] and the first MBT domain of L3MBTL [1OZ3] are overlaid.

Supplementary Table S1: **The Epigenetics pocketome.** Table S1A: 163 unique binding pockets included in this work. Table S1B: 575 PDB structures used in this work.

Kme Binding Pockets of Reader Domains

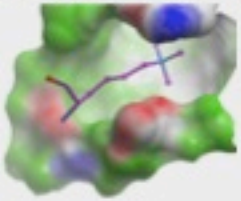

BAH [Kme]

CHROMO [Kme]

MBT [Kme]

PHD [Kme]

SPIN [Kme]

TUDOR [Kme/Rme]

PWWP [Kme]

YEATS [Kme]

Kme/Rme Binding Pockets of Enzymes

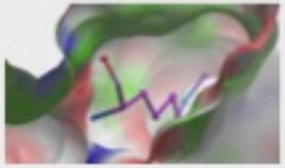

PMT [Kme/Rme]

KDM [Kme]

Kac Binding Pockets of Reader Domains

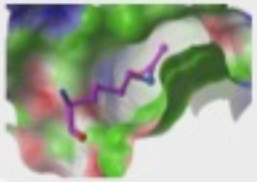

BROMO [Kac]

PMT [SAM]

DNMT [SAM]

RNMT [SAM]

S-adenosylmethionine Pockets

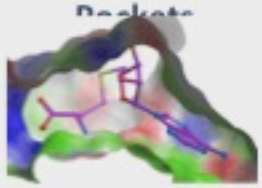

Acetyl-CoA Pockets

KAT [ac-CoA]

Kac Binding Pockets of Enzymes

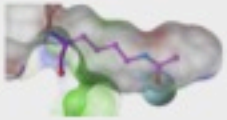

HDAC [Kac]

Nicot. Adenine Dinucleotide Pockets

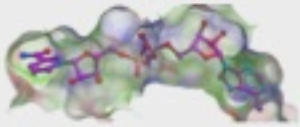

SIRT [NAD]

PMT [Allost.]

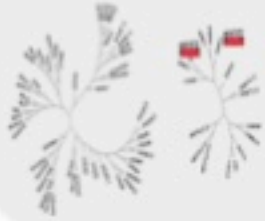

FIGURE 1

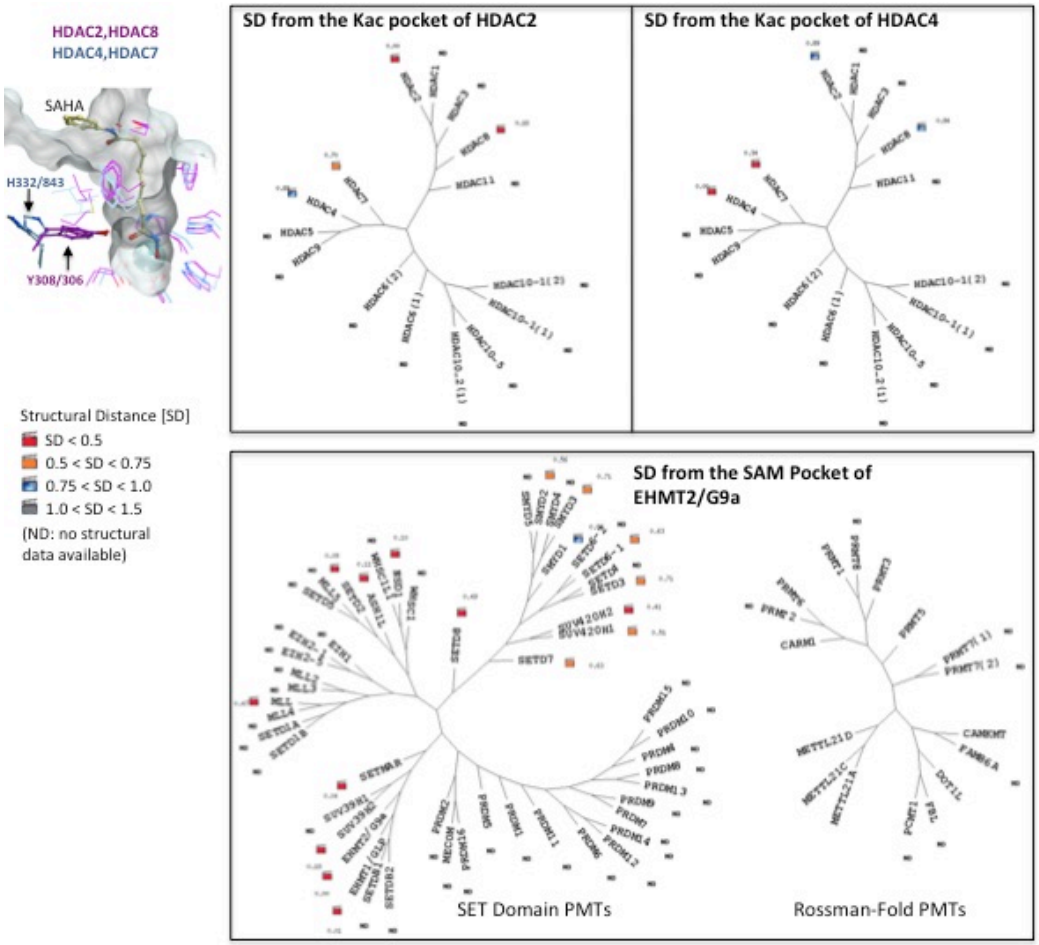
HDAC2,HDAC8
HDAC4,HDAC7
SAHA
H332/843
Y308/306
Structural Distance [SD]
SD < 0.5
0.5 < SD < 0.75
0.75 < SD < 1.0
1.0 < SD < 1.5
(ND: no structural data available)
SD from the Kac pocket of HDAC2
SD from the Kac pocket of HDAC4
SD from the SAM Pocket of EHMT2/G9a
SET Domain PMTs
Rossman-Fold PMTs

FIGURE 2

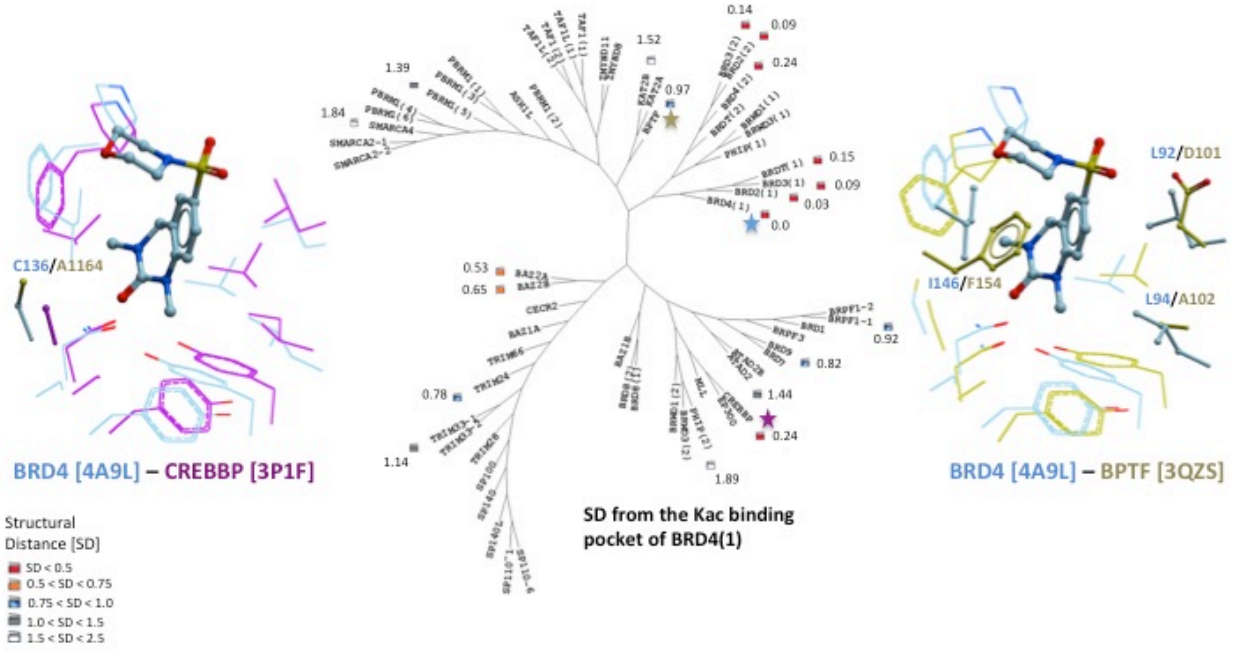
C136/A1164
BRD4 [4A9L] – CREBBP [3P1F]
Structural
Distance [SD]
SD < 0.5
0.5 < SD < 0.75
0.75 < SD < 1.0
1.0 < SD < 1.5
1.5 < SD < 2.5
SD from the Kac binding
pocket of BRD4(1)
L92/D101
I146/F154
L94/A102
BRD4 [4A9L] – BPTF [3QZS]

FIGURE 3

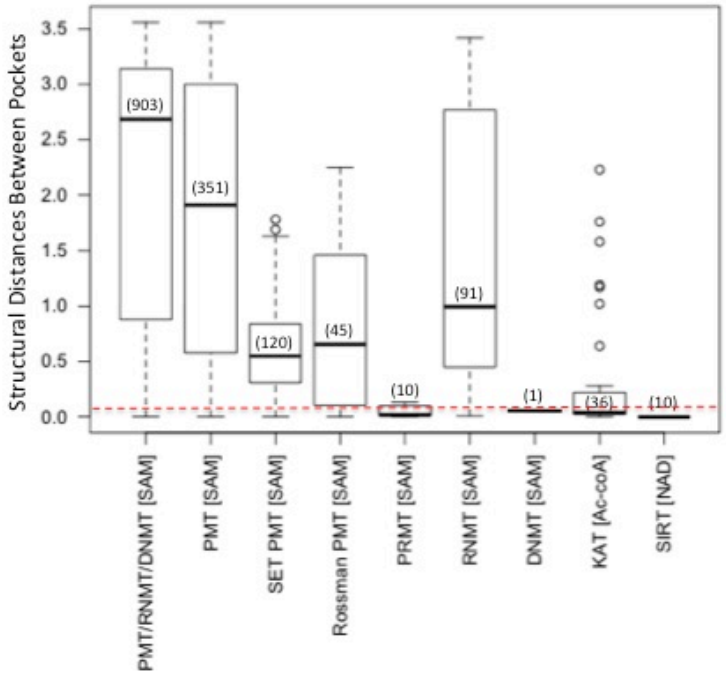
Structural Distances Between Pockets
3.5
3.0
2.5
2.0
1.5
1.0
0.5
0.0
(903)
(351)
(120)
(45)
(10)
(91)
(1)
(36)
(10)
PMT/RNMT/DNMT [SAM]
PMT [SAM]
SET PMT [SAM]
Rossman PMT [SAM]
PRMT [SAM]
RNMT [SAM]
DNMT [SAM]
KAT [Ac-coA]
SIRT [NAD]

FIGURE 4

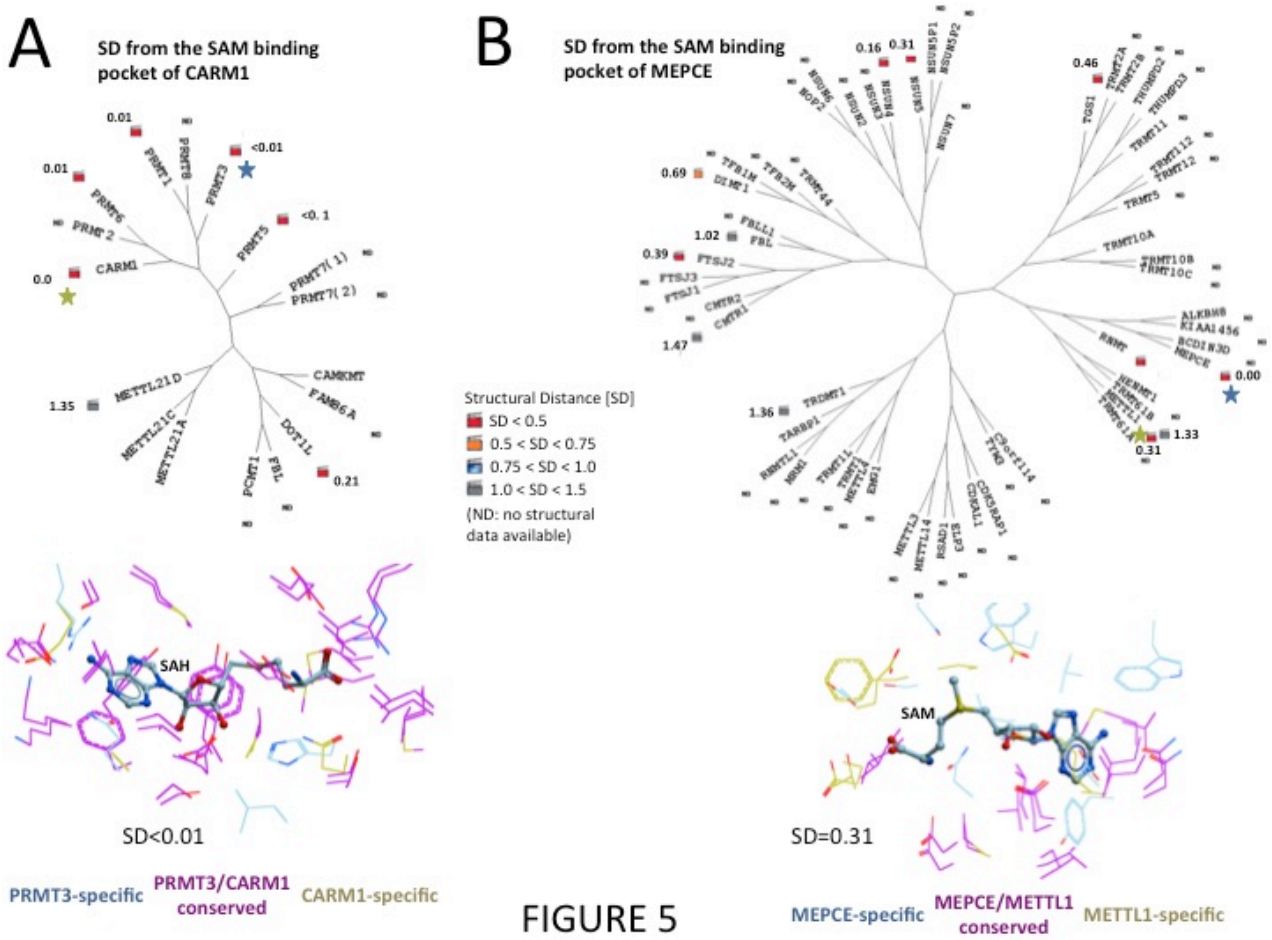
A
SD from the SAM binding pocket of CARM1
0.01
PRMT1
PRMT8
PRMT3
<0.01
0.01
PRMT6
PRMT2
CARM1
0.0
PRMT5
<0.1
PRMT7(1)
PRMT7(2)
CAMKMT
FAM86A
1.35
METTL21D
METTL21C
METTL21A
PCMT1
FBL
DOT1L
0.21
SAH
SD<0.01
PRMT3-specific
PRMT3/CARM1 conserved
CARM1-specific
B
SD from the SAM binding pocket of MEPCE
0.16
0.31
0.46
0.69
1.02
0.39
1.47
1.36
1.33
0.31
0.00
Structural Distance [SD]
SD < 0.5
0.5 < SD < 0.75
0.75 < SD < 1.0
1.0 < SD < 1.5
(ND: no structural data available)
SAM
SD=0.31
MEPCE-specific
MEPCE/METTL1 conserved
METTL1-specific

FIGURE 5

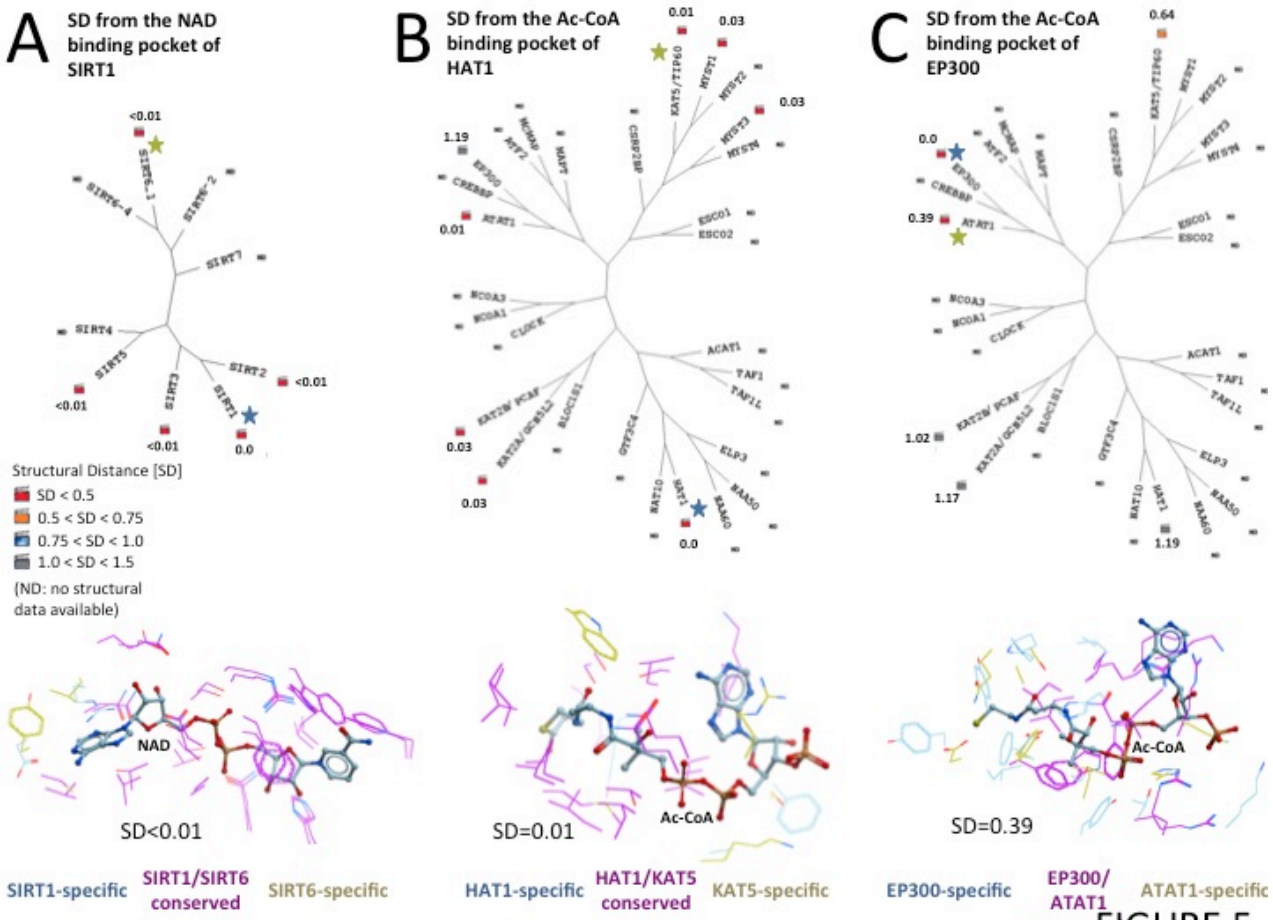
A
SD from the NAD binding pocket of SIRT1
<0.01
SIRT6-1
SIRT6-2
SIRT6-4
SIRT7
SIRT4
SIRT5
SIRT3
SIRT2
SIRT1
<0.01
<0.01
<0.01
<0.01
0.0
Structural Distance [SD]
SD < 0.5
0.5 < SD < 0.75
0.75 < SD < 1.0
1.0 < SD < 1.5
(ND: no structural data available)
NAD
SD<0.01
SIRT1-specific
SIRT1/SIRT6 conserved
SIRT6-specific
B
SD from the Ac-CoA binding pocket of HAT1
0.01
0.03
0.03
1.19
0.01
0.03
0.03
0.03
0.0
Ac-CoA
SD=0.01
HAT1-specific
HAT1/KAT5 conserved
KAT5-specific
C
SD from the Ac-CoA binding pocket of EP300
0.64
0.0
0.39
1.02
1.17
1.19
Ac-CoA
SD=0.39
EP300-specific
EP300/ ATAT1 conserved
ATAT1-specific

FIGURE 5

A

Pockets within 0.75 SD of the SAM binding pocket of active DOT1L

Gene	PDB	Distance	Substrate
DOT1L	1NW3	0	Protein
TGS1	3GDH	0.08	RNA
PRMT5	4GQB	0.23	Protein
CARM1	2Y1X	0.25	Protein
FTSJ2	2NYU	0.29	RNA
PRMT3	2FYT	0.31	Protein
PRMT1	1OR8	0.34	Protein
MEPCE	3CKK	0.39	RNA
DNMT1	3SWR	0.39	DNA
NSUN4	4FP9	0.4	RNA
DNMT3A	2QRV	0.42	DNA
DIMT1	1ZQ9	0.55	RNA
TRDMT1	1G55	0.57	RNA
NSUN5	2B9E	0.58	RNA
FBL	2IPX	0.61	RNA
METTL21C	4MTL	0.64	Protein
PRMT6	4HC4	0.72	Protein

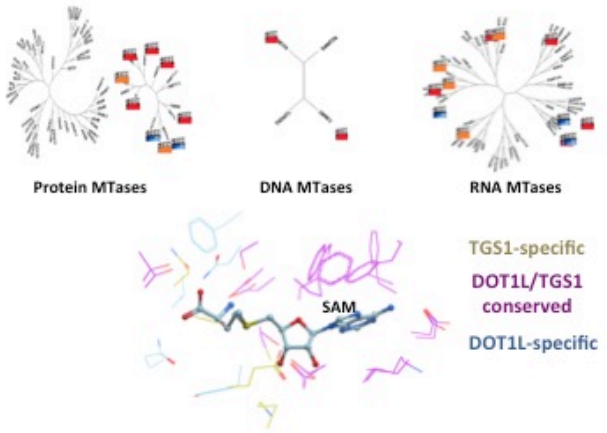

B

Pockets within 0.75 SD of the SAM binding pocket of inactive DOT1L

Gene	PDB	Distance	Substrate
DOT1L	4ER7	0	Protein
MEPCE	3G07	0.43	RNA
PRMT5	4GQB	0.44	Protein
TGS1	3GDH	0.55	RNA
METTL1	3CKK	0.62	RNA
PRMT1	1ORH	0.67	Protein
FTSJ2	2NYU	0.73	RNA
CARM1	2Y1X	0.74	Protein

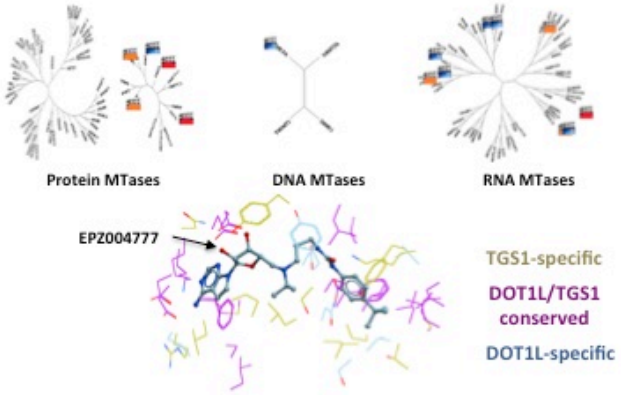

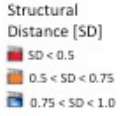

FIGURE 6

A

Pockets closest to the Rme2 binding site of SMNDC1 Tudor

Gene	PDB	Distance	Ligand
SMNDC1	4A4H	0	Rme2a
SMN1	4A4E	0.33	Rme2s
SND1	3OMG	1.41	Rme2s
TDRD3	2LTO	1.75	Rme2a
UHRF1	3DB3	1.78	Kme3
TP53BP1	2LVM	1.84	Kme2
CCDC101	3MEA	2.18	Kme3
PHF1	2M0O	2.29	Kme3
JMJD2A	2GFA	2.3	Kme3
MSL3L1	3OA6	2.38	Kme
PHF19	4BD3	2.42	Kme3

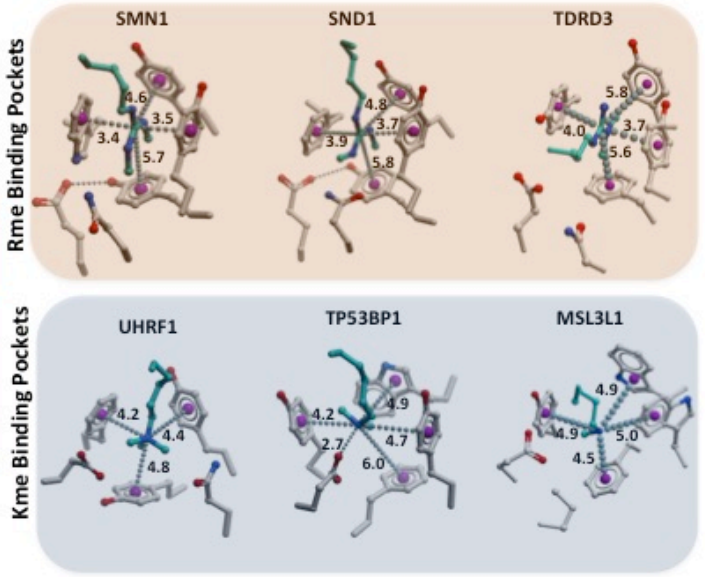

B

Pockets closest to the Kme3 binding site of UHRF1 Tudor

Domain	Gene	PDB	Distance	Ligand
TUDOR	UHRF1	4GY5	0	Kme3
1st MBT	L3MBTL	1OZ3	0.66	?
1st MBT	L3MBTL3	4FL6	0.92	?

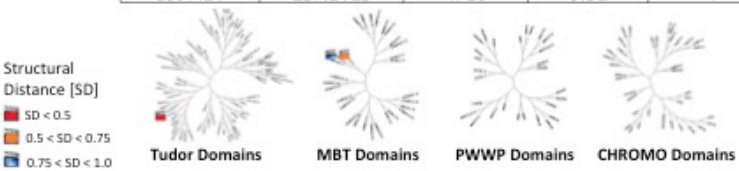

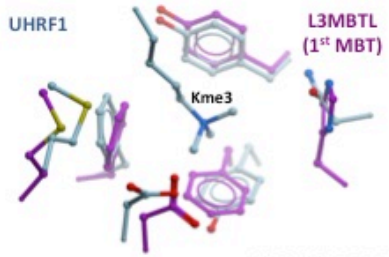

FIGURE 7

	family	gene	domain
1	ANKYRIN	EHMT1	1
2	BAH	DNMT1	1
3	BROMO	ATAD2	1
4	BROMO	BAZ2A	1
5	BROMO	BAZ2B	1
6	BROMO	BPTF	1
7	BROMO	BRD2	1
8	BROMO	BRD2	2
9	BROMO	BRD3	1
10	BROMO	BRD3	2
11	BROMO	BRD4	1
12	BROMO	BRD4	2
13	BROMO	BRD9	1
14	BROMO	BRDT	1
15	BROMO	BRPF1	1
16	BROMO	CREBBP	1
17	BROMO	KAT2B	1
18	BROMO	PBRM1	2
19	BROMO	PBRM1	5
20	BROMO	PHIP	2
21	BROMO	SMARCA4	1
22	BROMO	TRIM24	1
23	BROMO	TRIM33	1
24	CHROMO	CBX1	1
25	CHROMO	CBX2	1
26	CHROMO	CBX3	1
27	CHROMO	CBX5	1
28	CHROMO	CBX6	1
29	CHROMO	CBX7	1
30	CHROMO	CBX8	1
31	CHROMO	CHD1	1
32	CHROMO	MPHOSPH8	1
33	DNMTCof	DNMT1	1
34	DNMTCof	DNMT3A	1
35	HDAC	HDAC2	1
36	HDAC	HDAC4	1
37	HDAC	HDAC7	1
38	HDAC	HDAC8	1
39	KAT	ATA1	1
40	KAT	ATAT1	1
41	KAT	EP300	1
42	KAT	HAT1	1
43	KAT	KAT2A	1
44	KAT	KAT2B	1
45	KAT	KAT5	1
46	KAT	MYST1	1
47	KAT	MYST3	1
48	KATSubs	ATA1	1

49	KATSubs	EP300	1
50	KDM	JHDM1D	1
51	KDM	KDM2A	1
52	KDM	KDM4A	1
53	KDM	KDM4D	1
54	KDM	KDM4DL	1
55	KDM	KDM6A	1
56	KDM	KDM6B	1
57	KDM	NO66	1
58	KDM	PHF8	1
59	KDM	UTY	1
60	MBT	L3MBTL	1
61	MBT	L3MBTL	2
62	MBT	L3MBTL2	4
63	MBT	L3MBTL3	1
64	MBT	L3MBTL	3
65	MBT	L3MBTL3	2
66	MBT	SCML2	2
67	PHD	BAZ2A	1
68	PHD	BPTF	2
69	PHD	DIDO1	1
70	PHD	ING1	1
71	PHD	ING2	1
72	PHD	ING4	1
73	PHD	ING5	1
74	PHD	KDM5A	3
75	PHD	MLL	3
76	PHD	MLL5	1
77	PHD	PHF13	1
78	PHD	PHF2	1
79	PHD	PHF8	1
80	PHD	PYGO1	1
81	PHD	PYGO2	1
82	PHD	RAG2	1
83	PHD	TAF3	1
84	PHD	UHRF1	1
85	PMTAllo	PRMT3	1
86	PMTAllo	PRMT6	1
87	PMT	CARM1	1
88	PMTCof	ASH1L	1
89	PMTCof	CAMKMT	1
90	PMTCof	CARM1	1
91	PMTCof	DOT1L	1
92	PMTCof	EHMT1	1
93	PMTCof	EHMT2	1
94	PMTCof	METTL21A	1
95	PMTCof	METTL21C	1
96	PMTCof	METTL21D	1
97	PMTCof	MLL	1

98	PMTCof	NSD1	1
99	PMTCof	PRMT1	1
100	PMTCof	PRMT3	1
101	PMTCof	PRMT5	1
102	PMTCof	PRMT6	1
103	PMTCof	SETD2	1
104	PMTCof	SETD3	1
105	PMTCof	SETD6	1
106	PMTCof	SETD7	1
107	PMTCof	SETD8	1
108	PMTCof	SETMAR	1
109	PMTCof	SMYD1	1
110	PMTCof	SMYD2	1
111	PMTCof	SMYD3	1
112	PMTCof	SUV39H2	1
113	PMTCof	SUV420H1	1
114	PMTCof	SUV420H2	1
115	PMT	EHMT1	1
116	PMT	EHMT2	1
117	PMT	MLL	1
118	PMT	PRMT5	1
119	PMT	SETD2	1
120	PMT	SETD6	1
121	PMT	SETD7	1
122	PMT	SETD8	1
123	PMT	SMYD2	1
124	PMT	SUV420H2	1
125	PWWP	BRPF1	1
126	PWWP	HDGFRP2	1
127	PWWP	ZMYND11	1
128	RNMTCof	CMTR1	1
129	RNMTCof	DIMT1	1
130	RNMTCof	FBL	1
131	RNMTCof	FTSJ2	1
132	RNMTCof	MEPCE	1
133	RNMTCof	METTL1	1
134	RNMTCof	NSUN4	1
135	RNMTCof	NSUN5	1
136	RNMTCof	RNMT	1
137	RNMTCof	TARBP1	1
138	RNMTCof	TGS1	1
139	RNMTCof	TRDMT1	1
140	RNMTCof	TRMT10A	1
141	RNMTCof	TRMT61B	1
142	RNMT	TGS1	1
143	SIRT	SIRT1	1
144	SIRT	SIRT2	1
145	SIRT	SIRT3	1
146	SIRT	SIRT5	1

147	SIRT	SIRT6	1
148	SIRTSubs	SIRT2	1
149	SPINDLIN	SPIN1	1
150	SPINDLIN	SPIN1	2
151	SPINDLIN	SPIN4	1
152	TUDOR	CCDC101	2
153	TUDOR	JMJD2A	1
154	TUDOR	MSL3L1	1
155	TUDOR	PHF1	1
156	TUDOR	PHF19	1
157	TUDOR	SMN1	1
158	TUDOR	SMNDC1	1
159	TUDOR	SND1	1
160	TUDOR	TDRD3	1
161	TUDOR	TP53BP1	1
162	TUDOR	UHRF1	1
163	YEATS	MLLT3	1

	family	gene	domain	pdb	ligand
1	ANKYRIN	EHMT1	1	3B95	Kme2
2	BAH	DNMT1	1	3SWR	Kme2
3	BROMO	ATAD2	1	4QSP	Kac
4	BROMO	ATAD2	1	4QST	12q
5	BROMO	ATAD2	1	4QSV	thm
6	BROMO	ATAD2	1	4QSW	38t
7	BROMO	ATAD2	1	4QSX	38s
8	BROMO	ATAD2	1	4QUT	Kac
9	BROMO	ATAD2	1	4QUU	Kac
10	BROMO	ATAD2	1	4TYL	39o
11	BROMO	ATAD2	1	4TZ2	39r
12	BROMO	ATAD2	1	4TZ8	39u
13	BROMO	BAZ2A	1	4QBM	Kac
14	BROMO	BAZ2B	1	3Q2F	oam
15	BROMO	BAZ2B	1	4IR3	1fk
16	BROMO	BAZ2B	1	4IR5	ir5
17	BROMO	BAZ2B	1	4IR6	ir6
18	BROMO	BAZ2B	1	4NR9	Kac
19	BROMO	BAZ2B	1	4NRA	2lw
20	BROMO	BAZ2B	1	4NRB	2lx
21	BROMO	BAZ2B	1	4NRC	2ly
22	BROMO	BAZ2B	1	4QC1	Kac
23	BROMO	BAZ2B	1	4QC3	Kac
24	BROMO	BPTF	1	3QZS	Kac
25	BROMO	BPTF	1	3QZT	Kac
26	BROMO	BPTF	1	3QZV	Kac
27	BROMO	BRD2	1	2DVQ	Kac
28	BROMO	BRD2	1	2DVR	Kac
29	BROMO	BRD2	1	2DVS	Kac
30	BROMO	BRD2	1	2YDW	wsh
31	BROMO	BRD2	1	2YEK	eam
32	BROMO	BRD2	1	3AQA	byh
33	BROMO	BRD2	1	4A9E	3pf
34	BROMO	BRD2	1	4A9F	mb3
35	BROMO	BRD2	1	4A9H	tvp
36	BROMO	BRD2	1	4A9I	p9i
37	BROMO	BRD2	1	4A9J	tyl
38	BROMO	BRD2	1	4A9M	p9m
39	BROMO	BRD2	1	4A9N	a9n
40	BROMO	BRD2	1	4A9O	a9o
41	BROMO	BRD2	1	4A9P	a9p
42	BROMO	BRD2	1	4AKN	s5b
43	BROMO	BRD2	1	4ALG	1gh
44	BROMO	BRD2	1	4ALH	a9p
45	BROMO	BRD2	1	4UYF	73b
46	BROMO	BRD2	1	4UYH	9s3
47	BROMO	BRD2	2	2DVV	epe
48	BROMO	BRD2	2	3ONI	jq1

49	BROMO	BRD2	2	4J1P	1k0
50	BROMO	BRD2	2	4MR5	1k0
51	BROMO	BRD2	2	4MR6	1k0
52	BROMO	BRD2	2	4UYG	73b
53	BROMO	BRD3	1	2L5E	Kac
54	BROMO	BRD3	1	3S91	jq1
55	BROMO	BRD3	2	3S92	jq1
56	BROMO	BRD4	1	2YEL	wsh
57	BROMO	BRD4	1	3JVK	Kac
58	BROMO	BRD4	1	3MXF	jq1
59	BROMO	BRD4	1	3P5O	eam
60	BROMO	BRD4	1	3SVF	wdr
61	BROMO	BRD4	1	3SVG	odr
62	BROMO	BRD4	1	3U5J	08h
63	BROMO	BRD4	1	3U5K	08j
64	BROMO	BRD4	1	3U5L	08k
65	BROMO	BRD4	1	3UVW	Kac
66	BROMO	BRD4	1	3UVX	Kac
67	BROMO	BRD4	1	3UVY	Kac
68	BROMO	BRD4	1	3UW9	Kac
69	BROMO	BRD4	1	3ZYU	1gh
70	BROMO	BRD4	1	4A9L	p9l
71	BROMO	BRD4	1	4BJX	73b
72	BROMO	BRD4	1	4BW1	s5b
73	BROMO	BRD4	1	4BW2	uth
74	BROMO	BRD4	1	4BW3	9bm
75	BROMO	BRD4	1	4BW4	9b6
76	BROMO	BRD4	1	4C66	h4c
77	BROMO	BRD4	1	4C67	l5s
78	BROMO	BRD4	1	4CFK	ly2
79	BROMO	BRD4	1	4CFL	8dq
80	BROMO	BRD4	1	4DON	3pf
81	BROMO	BRD4	1	4.00E+96	0ns
82	BROMO	BRD4	1	4F3I	0s6
83	BROMO	BRD4	1	4GPJ	0q1
84	BROMO	BRD4	1	4HBV	15e
85	BROMO	BRD4	1	4HBW	14z
86	BROMO	BRD4	1	4HBX	14x
87	BROMO	BRD4	1	4HBY	13f
88	BROMO	BRD4	1	4HXK	1aj
89	BROMO	BRD4	1	4HXL	1a9
90	BROMO	BRD4	1	4HXM	1a8
91	BROMO	BRD4	1	4HXN	1a7
92	BROMO	BRD4	1	4HXO	1a6
93	BROMO	BRD4	1	4HXP	1a5
94	BROMO	BRD4	1	4HXR	1a4
95	BROMO	BRD4	1	4HXS	1a3
96	BROMO	BRD4	1	4IOQ	baq
97	BROMO	BRD4	1	4J0R	1h2

98	BROMO	BRD4	1	4J0S	1h3
99	BROMO	BRD4	1	4J3I	1k0
100	BROMO	BRD4	1	4KV1	Kac
101	BROMO	BRD4	1	4LR6	1xa
102	BROMO	BRD4	1	4LRG	1xb
103	BROMO	BRD4	1	4LYS	2sj
104	BROMO	BRD4	1	4LYW	21q
105	BROMO	BRD4	1	4LZR	loc
106	BROMO	BRD4	1	4LZS	l46
107	BROMO	BRD4	1	4MEN	25k
108	BROMO	BRD4	1	4MEO	25v
109	BROMO	BRD4	1	4MEP	24y
110	BROMO	BRD4	1	4MEQ	25o
111	BROMO	BRD4	1	4MR3	1k0
112	BROMO	BRD4	1	4MR4	1k0
113	BROMO	BRD4	1	4NQM	y1z
114	BROMO	BRD4	1	4NR8	2ll
115	BROMO	BRD4	1	4WIV	3p2
116	BROMO	BRD4	2	2LSP	Kac
117	BROMO	BRD4	2	2YEM	wsh
118	BROMO	BRD4	2	4KV4	Kac
119	BROMO	BRD9	1	4NQN	y1z
120	BROMO	BRDT	1	4FLP	jq1
121	BROMO	BRDT	1	4KCX	1qk
122	BROMO	BRPF1	1	2RS9	Kac
123	BROMO	BRPF1	1	4QYD	Kac
124	BROMO	BRPF1	1	4QYL	Kac
125	BROMO	BRPF1	1	4UYE	9f9
126	BROMO	CREBBP	1	1JSP	Kac
127	BROMO	CREBBP	1	2D82	ttr
128	BROMO	CREBBP	1	2L84	j28
129	BROMO	CREBBP	1	2L85	l85
130	BROMO	CREBBP	1	2RNY	Kac
131	BROMO	CREBBP	1	3P1C	Kac
132	BROMO	CREBBP	1	3P1D	mb3
133	BROMO	CREBBP	1	3P1F	3pf
134	BROMO	CREBBP	1	3SVH	krg
135	BROMO	CREBBP	1	4A9K	tyl
136	BROMO	CREBBP	1	4N3W	Kac
137	BROMO	CREBBP	1	4NR4	2lk
138	BROMO	CREBBP	1	4NR5	2ll
139	BROMO	CREBBP	1	4NR6	2ln
140	BROMO	CREBBP	1	4NR7	2lo
141	BROMO	CREBBP	1	4NYV	15e
142	BROMO	CREBBP	1	4NYW	2o3
143	BROMO	CREBBP	1	4NYX	2o4
144	BROMO	KAT2B	1	1JM4	Kac
145	BROMO	KAT2B	1	1WUG	np1
146	BROMO	KAT2B	1	1WUM	np2

147	BROMO	KAT2B	1	1ZS5	mib
148	BROMO	KAT2B	1	2RNW	Kac
149	BROMO	KAT2B	1	2RNX	Kac
150	BROMO	PBRM1	2	2KTB	Kac
151	BROMO	PBRM1	5	3MB4	mb3
152	BROMO	PBRM1	5	4Q0o	2xc
153	BROMO	PHIP	2	3MB3	mb3
154	BROMO	SMARCA4	1	3UVD	mb3
155	BROMO	TRIM24	1	3O34	Kac
156	BROMO	TRIM24	1	3O35	Kac
157	BROMO	TRIM24	1	3O36	Kac
158	BROMO	TRIM33	1	3U5O	Kac
159	BROMO	TRIM33	1	3U5P	Kac
160	CHROMO	CBX1	1	1GUW	Kme2
161	CHROMO	CBX2	1	3H91	Kme3
162	CHROMO	CBX3	1	2L11	Kme3
163	CHROMO	CBX3	1	3DM1	Kme3
164	CHROMO	CBX3	1	3TZD	Kme2
165	CHROMO	CBX5	1	3FDT	Kme3
166	CHROMO	CBX6	1	3GV6	Kme3
167	CHROMO	CBX6	1	3I90	Kme3
168	CHROMO	CBX7	1	2KVM	Kme2
169	CHROMO	CBX7	1	2L12	Kme3
170	CHROMO	CBX7	1	2L1B	Kme3
171	CHROMO	CBX8	1	3I91	Kme3
172	CHROMO	CHD1	1	2B2T	Kme3
173	CHROMO	CHD1	1	2B2U	Kme3
174	CHROMO	CHD1	1	2B2V	Kme1
175	CHROMO	CHD1	1	2B2W	Kme3
176	CHROMO	CHD1	1	4NW2	Kme3
177	CHROMO	CHD1	1	4O42	Kme2
178	CHROMO	MPHOSPH8	1	3QO2	Kme3
179	CHROMO	MPHOSPH8	1	3R93	Kme3
180	CHROMO	MPHOSPH8	1	3SVM	Kme4
181	DNMTCof	DNMT1	1	3PTA	SAH
182	DNMTCof	DNMT1	1	3SWR	SFG
183	DNMTCof	DNMT3A	1	2QRV	SAH
184	HDAC	HDAC2	1	3MAX	llx
185	HDAC	HDAC2	1	4LXZ	shh
186	HDAC	HDAC2	1	4LY1	20y
187	HDAC	HDAC4	1	2VQJ	tfg
188	HDAC	HDAC4	1	2VQM	ha3
189	HDAC	HDAC4	1	2VQO	tfg
190	HDAC	HDAC4	1	2VQQ	tfg
191	HDAC	HDAC4	1	2VQV	ha3
192	HDAC	HDAC4	1	4CBT	9f4
193	HDAC	HDAC4	1	4CBY	kee
194	HDAC	HDAC7	1	3C10	tsn
195	HDAC	HDAC7	1	3ZNR	nu9

196	HDAC	HDAC7	1	3ZNS	nu7
197	HDAC	HDAC8	1	1T64	tsn
198	HDAC	HDAC8	1	1T67	b3n
199	HDAC	HDAC8	1	1T69	shh
200	HDAC	HDAC8	1	1VKG	cri
201	HDAC	HDAC8	1	1W22	nhb
202	HDAC	HDAC8	1	2V5W	Kac
203	HDAC	HDAC8	1	2V5X	v5x
204	HDAC	HDAC8	1	3EW8	b3n
205	HDAC	HDAC8	1	3EWF	Kac
206	HDAC	HDAC8	1	3EZP	b3n
207	HDAC	HDAC8	1	3EZT	b3n
208	HDAC	HDAC8	1	3F06	b3n
209	HDAC	HDAC8	1	3F07	age
210	HDAC	HDAC8	1	3F0R	tsn
211	HDAC	HDAC8	1	3MZ3	b3n
212	HDAC	HDAC8	1	3MZ4	b3n
213	HDAC	HDAC8	1	3MZ6	b3n
214	HDAC	HDAC8	1	3MZ7	b3n
215	HDAC	HDAC8	1	3RQD	02g
216	HDAC	HDAC8	1	3SFF	0di
217	HDAC	HDAC8	1	3SFH	1di
218	KAT	ATA1	1	4PK2	COA
219	KAT	ATA1	1	4PK3	COA
220	KAT	ATAT1	1	3VWD	ACO
221	KAT	ATAT1	1	3VWE	COA
222	KAT	ATAT1	1	4B5P	ACO
223	KAT	ATAT1	1	4GS4	ACO
224	KAT	EP300	1	3BIY	01k
225	KAT	EP300	1	4PZR	COA
226	KAT	EP300	1	4PZS	ACO
227	KAT	EP300	1	4PZT	sop
228	KAT	HAT1	1	2P0W	ACO
229	KAT	KAT2A	1	1Z4R	ACO
230	KAT	KAT2B	1	4NSQ	COA
231	KAT	KAT5	1	2OU2	ACO
232	KAT	MYST1	1	2GIV	ACO
233	KAT	MYST1	1	2PQ8	COA
234	KAT	MYST3	1	2OZU	ACO
235	KAT	MYST3	1	2RC4	ACO
236	KATSubs	ATA1	1	4PK2	Kac
237	KATSubs	ATA1	1	4PK3	Kac
238	KATSubs	EP300	1	4BHW	01k
239	KDM	JHDM1D	1	3U78	e67
240	KDM	KDM2A	1	4QWN	Kme3
241	KDM	KDM2A	1	4QX7	Kme2
242	KDM	KDM2A	1	4QX8	Kme3
243	KDM	KDM2A	1	4QXB	Kme3
244	KDM	KDM2A	1	4QXC	Kme2

245	KDM	KDM2A	1	4QXH	Kme
246	KDM	KDM4A	1	2OQ6	Kme3
247	KDM	KDM4A	1	2OS2	Kme3
248	KDM	KDM4A	1	2OT7	Kme1
249	KDM	KDM4A	1	2OX0	Kme4
250	KDM	KDM4A	1	2P5B	Kme3
251	KDM	KDM4A	1	2PXJ	Kme1
252	KDM	KDM4A	1	2Q8C	Kme3
253	KDM	KDM4A	1	2Q8D	Kme2
254	KDM	KDM4A	1	2Q8E	Kme3
255	KDM	KDM4A	1	2VD7	pd2
256	KDM	KDM4A	1	2WWJ	y28
257	KDM	KDM4A	1	2YBP	Kme3
258	KDM	KDM4A	1	2YBS	Kme3
259	KDM	KDM4A	1	3NJY	8xq
260	KDM	KDM4A	1	3PDQ	kc6
261	KDM	KDM4A	1	3RVH	hq2
262	KDM	KDM4A	1	3U4S	Kme3
263	KDM	KDM4A	1	4AI9	dza
264	KDM	KDM4A	1	4BIS	8hq
265	KDM	KDM4A	1	4GD4	0ws
266	KDM	KDM4A	1	4V2V	Kme3
267	KDM	KDM4D	1	4HON	Kme3
268	KDM	KDM4DL	1	2W2I	pd2
269	KDM	KDM6A	1	3AVR	Kme3
270	KDM	KDM6A	1	3ZPO	k0i
271	KDM	KDM6B	1	2XXZ	8xq
272	KDM	NO66	1	4DIQ	pd2
273	KDM	PHF8	1	3KV4	Kme2
274	KDM	PHF8	1	4DO0	dza
275	KDM	UTY	1	3ZPO	k0i
276	MBT	L3MBTL	1	1OYX	mes
277	MBT	L3MBTL	1	1OZ3	mes
278	MBT	L3MBTL	2	1OYX	mes
279	MBT	L3MBTL	2	1OZ3	mes
280	MBT	L3MBTL	2	2PQW	Kme2
281	MBT	L3MBTL	2	2RHI	Kme2
282	MBT	L3MBTL	2	2RHU	Kme2
283	MBT	L3MBTL	2	2RHX	Kme2
284	MBT	L3MBTL	2	2RHY	Kme1
285	MBT	L3MBTL	2	2RJC	mes
286	MBT	L3MBTL	2	2RJE	Kme2
287	MBT	L3MBTL	2	2RJF	Kme2
288	MBT	L3MBTL	2	3OQ5	Kme1
289	MBT	L3MBTL	2	3P8H	p8h
290	MBT	L3MBTL	2	3UWN	uwn
291	MBT	L3MBTL2	4	3F70	Kme1
292	MBT	L3MBTL3	1	4FL6	uwn
293	MBT	L3MBTL3	1	4L59	1vz

294	MBT	L3MBTL	3	1OZ2	mes
295	MBT	L3MBTL3	2	3UT1	epe
296	MBT	L3MBTL3	2	4FL6	uwn
297	MBT	L3MBTL	3	2RJC	mes
298	MBT	SCML2	2	2VYT	Kme1
299	MBT	SCML2	2	4EDU	Kme1
300	PHD	BAZ2A	1	4Q6F	K
301	PHD	BPTF	2	2F6J	Kme3
302	PHD	BPTF	2	2FSA	Kme2
303	PHD	BPTF	2	2FUU	Kme3
304	PHD	BPTF	2	2RI7	Kme2
305	PHD	DIDO1	1	4L7X	Kme3
306	PHD	ING1	1	2QIC	Kme3
307	PHD	ING2	1	2G6Q	Kme3
308	PHD	ING4	1	2PNX	Kme3
309	PHD	ING4	1	2VNF	Kme3
310	PHD	ING5	1	3C6W	Kme3
311	PHD	KDM5A	3	2KGI	Kme3
312	PHD	KDM5A	3	3GL6	Kme3
313	PHD	MLL	3	3LQI	Kme2
314	PHD	MLL	3	3LQJ	Kme3
315	PHD	MLL5	1	4L58	Kme3
316	PHD	PHF13	1	3O7A	Kme3
317	PHD	PHF2	1	3KQI	Kme3
318	PHD	PHF8	1	3KV4	Kme3
319	PHD	PYGO1	1	2VPE	Kme2
320	PHD	PYGO1	1	2VPG	Kme2
321	PHD	PYGO1	1	2YYR	Kme3
322	PHD	PYGO2	1	4UP0	Kme2
323	PHD	RAG2	1	2V83	Kme3
324	PHD	RAG2	1	2V85	Kme3
325	PHD	RAG2	1	2V86	Kme3
326	PHD	RAG2	1	2V87	Kme3
327	PHD	RAG2	1	2V88	Kme2
328	PHD	RAG2	1	2V89	Kme3
329	PHD	TAF3	1	2K17	Kme3
330	PHD	UHRF1	1	3SOW	Kme3
331	PMTAllo	PRMT3	1	3SMQ	tdu
332	PMTAllo	PRMT3	1	4HSG	ktd
333	PMTAllo	PRMT3	1	4QQN	3bq
334	PMTAllo	PRMT6	1	4QPP	36s
335	PMT	CARM1	1	2Y1W	849
336	PMT	CARM1	1	2Y1X	845
337	PMT	CARM1	1	4IKP	4ik
338	PMTCof	ASH1L	1	3OPE	SAM
339	PMTCof	CAMKMT	1	4PWY	SAH
340	PMTCof	CARM1	1	2V74	SAH
341	PMTCof	CARM1	1	2Y1W	SFG
342	PMTCof	CARM1	1	2Y1X	SAH

343	PMTCof	CARM1	1	3B3F	SAH
344	PMTCof	CARM1	1	4IKP	4ik
345	PMTCof	DOT1L	1	1NW3	SAM
346	PMTCof	DOT1L	1	3QOW	SAM
347	PMTCof	DOT1L	1	3QOX	SAH
348	PMTCof	DOT1L	1	3SR4	tt8
349	PMTCof	DOT1L	1	3SX0	sx0
350	PMTCof	DOT1L	1	3UWP	5id
351	PMTCof	DOT1L	1	4EK9	ep4
352	PMTCof	DOT1L	1	4EKG	0qj
353	PMTCof	DOT1L	1	4EKI	0qk
354	PMTCof	DOT1L	1	4EQZ	aw0
355	PMTCof	DOT1L	1	4ER0	aw1
356	PMTCof	DOT1L	1	4ER3	0qk
357	PMTCof	DOT1L	1	4ER5	0qk
358	PMTCof	DOT1L	1	4ER6	aw2
359	PMTCof	DOT1L	1	4ER7	aw3
360	PMTCof	DOT1L	1	4HRA	ep6
361	PMTCof	EHMT1	1	2IGQ	SAH
362	PMTCof	EHMT1	1	2RFI	SAH
363	PMTCof	EHMT1	1	3FPD	SAH
364	PMTCof	EHMT1	1	3HNA	SAH
365	PMTCof	EHMT1	1	3MO0	SAH
366	PMTCof	EHMT1	1	3SW9	SFG
367	PMTCof	EHMT1	1	3SWC	SAH
368	PMTCof	EHMT1	1	4H4H	SAH
369	PMTCof	EHMT1	1	4I51	SAH
370	PMTCof	EHMT2	1	2O8J	SAH
371	PMTCof	EHMT2	1	3K5K	SAH
372	PMTCof	EHMT2	1	3RJW	SAH
373	PMTCof	EHMT2	1	4NVQ	SAH
374	PMTCof	METTL21A	1	4LEC	SAH
375	PMTCof	METTL21C	1	4MTL	SAH
376	PMTCof	METTL21D	1	4LG1	SAM
377	PMTCof	MLL	1	2W5Y	SAH
378	PMTCof	MLL	1	2W5Z	SAH
379	PMTCof	NSD1	1	3OOI	SAM
380	PMTCof	PRMT1	1	1OR8	SAH
381	PMTCof	PRMT1	1	1ORH	SAH
382	PMTCof	PRMT1	1	1ORI	SAH
383	PMTCof	PRMT1	1	3Q7E	SAH
384	PMTCof	PRMT3	1	2FYT	SAH
385	PMTCof	PRMT5	1	4GQB	0xu
386	PMTCof	PRMT6	1	4HC4	SAH
387	PMTCof	PRMT6	1	4QQK	37h
388	PMTCof	SETD2	1	4FMU	0um
389	PMTCof	SETD2	1	4H12	SAH
390	PMTCof	SETD3	1	3SMT	SAM
391	PMTCof	SETD6	1	3QXY	SAM

392	PMTCof	SETD6	1	3RC0	SAM
393	PMTCof	SETD7	1	1MT6	SAH
394	PMTCof	SETD7	1	1N6A	SAM
395	PMTCof	SETD7	1	1N6C	SAM
396	PMTCof	SETD7	1	1O9S	SAH
397	PMTCof	SETD7	1	1XQH	SAH
398	PMTCof	SETD7	1	2F69	SAH
399	PMTCof	SETD7	1	3CBM	SAH
400	PMTCof	SETD7	1	3CBO	SAH
401	PMTCof	SETD7	1	3CBP	SFG
402	PMTCof	SETD7	1	3M53	SAH
403	PMTCof	SETD7	1	3M54	SAH
404	PMTCof	SETD7	1	3M55	SAH
405	PMTCof	SETD7	1	3M56	SAH
406	PMTCof	SETD7	1	3M57	SAH
407	PMTCof	SETD7	1	3M58	SAH
408	PMTCof	SETD7	1	3M59	SAH
409	PMTCof	SETD7	1	3M5A	SAH
410	PMTCof	SETD7	1	3OS5	SAH
411	PMTCof	SETD7	1	3VUZ	k15
412	PMTCof	SETD7	1	3VV0	kh3
413	PMTCof	SETD7	1	4E47	SAM
414	PMTCof	SETD7	1	4J7F	SAH
415	PMTCof	SETD7	1	4J7I	SAH
416	PMTCof	SETD7	1	4J83	SAM
417	PMTCof	SETD7	1	4J8O	SAH
418	PMTCof	SETD7	1	4JDS	SAM
419	PMTCof	SETD7	1	4JLG	SAM
420	PMTCof	SETD8	1	1ZKK	SAH
421	PMTCof	SETD8	1	2BQZ	SAH
422	PMTCof	SETD8	1	3F9W	SAH
423	PMTCof	SETD8	1	3F9X	SAH
424	PMTCof	SETD8	1	3F9Y	SAH
425	PMTCof	SETD8	1	3F9Z	SAH
426	PMTCof	SETD8	1	4IJ8	SAM
427	PMTCof	SETMAR	1	3BO5	SAH
428	PMTCof	SMYD1	1	3N71	SFG
429	PMTCof	SMYD2	1	3RIB	SAH
430	PMTCof	SMYD2	1	3S7B	SAM
431	PMTCof	SMYD2	1	3S7D	SAH
432	PMTCof	SMYD2	1	3S7F	SAM
433	PMTCof	SMYD2	1	3S7J	SAM
434	PMTCof	SMYD2	1	3TG4	SAM
435	PMTCof	SMYD2	1	3TG5	SAH
436	PMTCof	SMYD2	1	4O6F	SAH
437	PMTCof	SMYD3	1	3MEK	SAM
438	PMTCof	SMYD3	1	3OXF	SAH
439	PMTCof	SMYD3	1	3OXG	SAH
440	PMTCof	SMYD3	1	3OXL	SAH

441	PMTCof	SMYD3	1	3PDN	SFG
442	PMTCof	SMYD3	1	3QWP	SAM
443	PMTCof	SMYD3	1	3RU0	SFG
444	PMTCof	SUV39H2	1	2R3A	SAM
445	PMTCof	SUV420H1	1	3S8P	SAM
446	PMTCof	SUV420H1	1	4BUP	SAM
447	PMTCof	SUV420H2	1	3RQ4	SAM
448	PMTCof	SUV420H2	1	4AU7	SAH
449	PMT	EHMT1	1	2RFI	Kme2
450	PMT	EHMT1	1	3FPD	q4a
451	PMT	EHMT1	1	3HNA	Kme1
452	PMT	EHMT1	1	3MO2	e67
453	PMT	EHMT1	1	3MO5	e72
454	PMT	EHMT2	1	3K5K	dxq
455	PMT	EHMT2	1	3RJW	ciq
456	PMT	EHMT2	1	4NVQ	2od
457	PMT	MLL	1	2W5Z	Kme2
458	PMT	PRMT5	1	4GQB	R
459	PMT	SETD2	1	4FMU	0um
460	PMT	SETD6	1	3RC0	K
461	PMT	SETD7	1	1O9S	Kme1
462	PMT	SETD7	1	1XQH	Kme1
463	PMT	SETD7	1	2F69	Kme1
464	PMT	SETD7	1	3CBM	Kme1
465	PMT	SETD7	1	3CBO	Kme1
466	PMT	SETD7	1	3M55	Kme1
467	PMT	SETD7	1	3M56	Kme2
468	PMT	SETD7	1	3M58	Kme1
469	PMT	SETD7	1	3M59	Kme2
470	PMT	SETD7	1	3M5A	Kme3
471	PMT	SETD7	1	3OS5	Kme1
472	PMT	SETD7	1	3VUZ	k15
473	PMT	SETD7	1	3VV0	kh3
474	PMT	SETD7	1	4E47	0n6
475	PMT	SETD7	1	4JDS	1l4
476	PMT	SETD7	1	4JLG	1l8
477	PMT	SETD8	1	2BQZ	Kme1
478	PMT	SETD8	1	3F9X	Kme2
479	PMT	SETD8	1	3F9Y	Kme1
480	PMT	SMYD2	1	3S7B	nh5
481	PMT	SMYD2	1	3S7D	Kme1
482	PMT	SUV420H2	1	4AU7	Kme2
483	PWWP	BRPF1	1	2X4W	Kme3
484	PWWP	BRPF1	1	2X4X	Kme3
485	PWWP	BRPF1	1	2X4Y	Kme3
486	PWWP	BRPF1	1	3MO8	Kme3
487	PWWP	HDGFRP2	1	3QJ6	Kme3
488	PWWP	ZMYND11	1	4N4H	Kme3
489	PWWP	ZMYND11	1	4N4I	Kme3

490	RNMTCof	CMTR1	1	4N48	SAM
491	RNMTCof	CMTR1	1	4N49	SAM
492	RNMTCof	DIMT1	1	1ZQ9	SAM
493	RNMTCof	FBL	1	2IPX	mta
494	RNMTCof	FTSJ2	1	2NYU	SAM
495	RNMTCof	MEPCE	1	3G07	SAM
496	RNMTCof	METTL1	1	3CKK	SAM
497	RNMTCof	NSUN4	1	4FP9	SAM
498	RNMTCof	NSUN4	1	4FZV	SAM
499	RNMTCof	NSUN5	1	2B9E	SAM
500	RNMTCof	RNMT	1	3BGV	SAH
501	RNMTCof	RNMT	1	3EPP	SFG
502	RNMTCof	TARBP1	1	2HA8	SAH
503	RNMTCof	TGS1	1	3EGI	adp
504	RNMTCof	TGS1	1	3GDH	SAH
505	RNMTCof	TRDMT1	1	1G55	SAH
506	RNMTCof	TRMT10A	1	4FMW	SAH
507	RNMTCof	TRMT61B	1	2B25	SAM
508	RNMT	TGS1	1	3GDH	mgp
509	SIRT	SIRT1	1	4I5I	NAD
510	SIRT	SIRT1	1	4IF6	APR
511	SIRT	SIRT1	1	4KXQ	APR
512	SIRT	SIRT2	1	3ZGV	AR6
513	SIRT	SIRT3	1	4BN4	AR6
514	SIRT	SIRT3	1	4BN5	CNA
515	SIRT	SIRT3	1	4BN5	sr7
516	SIRT	SIRT3	1	4BV3	NAD
517	SIRT	SIRT3	1	4BVB	AR6
518	SIRT	SIRT3	1	4BVG	oad
519	SIRT	SIRT3	1	4BVH	oad
520	SIRT	SIRT3	1	4FVT	CNA
521	SIRT	SIRT3	1	4JSR	1nq
522	SIRT	SIRT3	1	4JT8	1nr
523	SIRT	SIRT3	1	4JT9	1ns
524	SIRT	SIRT5	1	2B4Y	APR
525	SIRT	SIRT5	1	2B4Y	epe
526	SIRT	SIRT5	1	2NYR	svr
527	SIRT	SIRT5	1	3RIY	NAD
528	SIRT	SIRT5	1	4F56	cgk
529	SIRT	SIRT5	1	4G1C	CNA
530	SIRT	SIRT6	1	3K35	APR
531	SIRT	SIRT6	1	3PKI	AR6
532	SIRT	SIRT6	1	3PKJ	a2n
533	SIRT	SIRT6	1	3ZG6	APR
534	SIRTSubs	SIRT2	1	4L3O	Kac
535	SPINDLIN	SPIN1	1	4H75	nhe
536	SPINDLIN	SPIN1	1	4MZF	Rme2a
537	SPINDLIN	SPIN1	2	4H75	Kme3
538	SPINDLIN	SPIN1	2	4MZF	Kme3

539	SPINDLIN	SPIN1	2	4MZG	Kme3
540	SPINDLIN	SPIN1	2	4MZH	Kme3
541	SPINDLIN	SPIN4	1	4UY4	Kme3
542	TUDOR	CCDC101	2	3ME9	Kme3
543	TUDOR	CCDC101	2	3MEA	Kme3
544	TUDOR	CCDC101	2	3MET	Kme2
545	TUDOR	CCDC101	2	3MEU	Kme3
546	TUDOR	CCDC101	2	3MEV	Kme3
547	TUDOR	JMJD2A	1	2GFA	Kme3
548	TUDOR	JMJD2A	1	2QQS	Kme3
549	TUDOR	MSL3L1	1	3OA6	Kme1
550	TUDOR	MSL3L1	1	3OB9	nhe
551	TUDOR	PHF1	1	2M0O	Kme3
552	TUDOR	PHF1	1	4HCZ	Kme3
553	TUDOR	PHF19	1	4BD3	Kme3
554	TUDOR	SMN1	1	4A4E	Rme2s
555	TUDOR	SMN1	1	4A4G	Rme2a
556	TUDOR	SMN1	1	4QQ6	36X
557	TUDOR	SMNDC1	1	4A4F	Rme2s
558	TUDOR	SMNDC1	1	4A4H	Rme2a
559	TUDOR	SND1	1	3OMC	Rme2s
560	TUDOR	SND1	1	3OMG	Rme2s
561	TUDOR	TDRD3	1	2LTO	Rme2a
562	TUDOR	TP53BP1	1	2IG0	Kme2
563	TUDOR	TP53BP1	1	2LVM	Kme2
564	TUDOR	TP53BP1	1	3LGF	Kme2
565	TUDOR	TP53BP1	1	3LGL	Kme2
566	TUDOR	TP53BP1	1	3LH0	Kme2
567	TUDOR	TP53BP1	1	4CRI	Kme2
568	TUDOR	TP53BP1	1	4RG2	3OO
569	TUDOR	UHRF1	1	2L3R	Kme3
570	TUDOR	UHRF1	1	3ASK	Kme3
571	TUDOR	UHRF1	1	3DB3	Kme3
572	TUDOR	UHRF1	1	4GY5	Kme3
573	TUDOR	UHRF1	1	4QQD	36X
574	TUDOR	UHRF1	1	4QQD	36X
575	YEATS	MLLT3	1	4TMP	Kac